Dual band, Miniaturized Permittivity Measurement Sensor with Negative-Order SIW Resonator

P. Mohammadi, H. Teimouri, A. Mohammadi, *Member*, IEEE, S. Demir, *Member, IEEE,* and A. Kara, Senior *Member, IEEE*

***Abstract*—A novel dual band, highly sensitive Substrate Integrated Waveguide (SIW) sensor for permittivity measurements is presented. A pair of modified Complementary Split Ring Resonators (CSRRs) is etched on SIW surface. CSRRs are located in the center of SIW, where the electric field distribution is high so that the coupling be maximized. The coupling between the SIW and the CSRRs as well as the adjacent CSRRs results in two notches in transmission coefficient. These notches vary with the dielectric loading on the sensor. The ratio of notch variation to the load permittivity variation determines the sensitivity of proposed sensor. Two sensitivities proportional to two notches are provided. Normalized sensitivities from both notches show identical values. Therefore, any environmental effect have the same impact on the TZs. This demonstrates the potential of the proposed sensor for differential operation that can mitigate the effect of environmental conditions. The size of the proposed sensor is small as the inductive and the capacitive effects of CSRRs forced the SIW to operate below the cut off frequency at negative-order-resonance mode. All design steps including SIW design, CSRRs design and modified CSRRs effects are presented in details. The sensor operation principle is described through its equivalent circuit model and simulation results. The experimental results indicates that the normalized sensitivity is 3.4%, which is much higher than similar sensors. The prototype sensor size (27.8×18.4×0.508 mm^3) is smaller than those reported in the literature.**

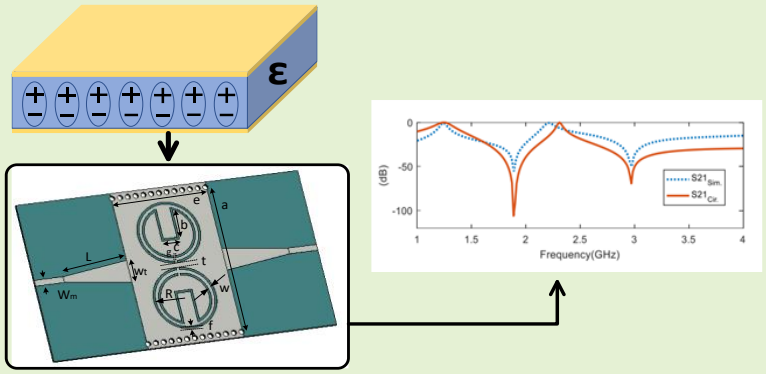

***Index Terms*—CSRR, highly sensitive, microwave sensor, small size, SIW.**

I. Introduction

NONE-DESTRUCTIVE characterization of material permittivity has many applications [1,2]. Microwave-based methods for non-destructive applications provide higher accuracy and real-time performance, which is an outstanding feature in comparison with other methods. Microwave sensors have excellent performance owing to design flexibility on Printed Circuit Board (PCB), easy fabrication, low cost as well as integration with other planar components. In available microwave sensors, the host consists of microstrip lines [3-5] or Substrate Integrated Waveguides (SIW) [6-7]. Usually Split Ring resonator (SRR) or Complementary Split Ring Resonator (CSRR) are loaded to the host and provide resonance condition, which leads to strong electric or magnetic fields concentrations around SRR or CSRR. Therefore, any variation in these fields, results in corresponding changes in resonant or transmission frequencies of these structures. SIW is a popular guided-wave structure due to high density integration with planar integrated circuits, high Q, low cost and low loss [8-9]. In [10], dielectric properties of substrate materials are characterized with modified SIW cavity. Enhanced SIW two-port sensor for material characterization is presented in [11], which shows low sensitivity due to limited penetration of electromagnetic field in material under test (MUT). An SIW temperature sensor for harsh environment and a tunable SIW sensor for liquid permittivity measurement are reported in [12] and [13], respectively. Hydrogen sensing based on SIW phase shifter [14] has a large operation frequency variation. Accurate permittivity estimation with a newly fed enhanced SIW sensor is achieved in [15]. CSRR is loaded on SIW for crack detection [16] and rotation measurement [17]. A dielectric permittivity detection sensor based on SIW with negative order resonance is reported in [18-19], which shows a significant level of miniaturization. Negative-Order-Resonance appears due to inductive and

P. Mohammadi is with the Department of Electrical Engineering, Urmia Branch, Islamic Azad University, Urmia, Iran.(e-mail: p.mohammadi@ iaurmia.ac.ir).
H.Teimouri is with the Department of Electrical Engineering, Urmia Branch, Islamic Azad University, Urmia, Iran.(e-mail: hadi.teimouri@yahoo.com)
A. Mohammadi is with Department of Electrical and Electronic Engineering, University of Bath.(e-mail: a.mohammadi@bath.ac.uk).
S. Demir is with Department of Electrical and Electronics Engineering Middle East Technical University.(e-mail: simsek@metu.edu.tr).
A. Kara is with the Department of Electrical and Electronics Engineering, Faculty of Engineering, Gazi University, Ankara 06570, Turkey(e-mail: akara@gazi.edu.tr).

capacitive effects of CSRRs, where the SIW operates below the cutoff frequency of its equivalent waveguide. Therefore, operation frequency and transmission zeros are decreased. Generally decreasing the operation frequency, can be achieved by increasing the size of SIW, therefore size reduction is another result of CSRRs loaded on SIW, which will be explained in the next section. In most of available SIW sensors, the effect of CSRR on the size of the structure and also, dual band operation has not been investigated. In the proposed sensor, a novel SIW sensor loaded with modified CSRRs is presented. In order to minimize the size of sensor, CSRRs are loaded in the middle part of SIW, where the electric filed is maximum. The proposed design improves the sensitivity by extended CSRRs with rectangular split extension. This also provides dual band operation.

Microwave sensors are sensitive to change in surrounding conditions, since the electromagnetic propagation is also susceptible to permittivity change [21]. Dual band sensors can overcome this drawback. In dual resonant response for humidity elimination [22] two distinct resonators are implemented. One is constant to variation of MUT and the other is dynamic to MUT variation. However, the reported sensitivity is low. In [23] dual band operation is realized with two CSRRs, where variation in material properties affect both band resonators. This study did not address the environmental conditions. In [24] an attempt has been made to cancel temperature variations but the structures suffer from complexity caused by using two quarter ring resonator sensors. Dual notch microwave sensor based on complementary resonator for permittivity detection is reported in [25]. Differential operation is also investigated in dual band sensors [26-27]. In [25] two microstrip line is loaded with CSRRs. Symmetrical loading results in a single band stop notch in the transmission response, whereas asymmetrical loadings lead to double notches. The sensitivity of this sensor is influenced by the length of transmission line. A similar study is designed in [26] for microfluidic sensitivity. In [27] step impedance resonators (SIPs) are used, however, the inductance between two SIRs affects the sensitivity.

In the proposed sensor the theoretical sensitivity of two bands is identical. Therefore, variations in surrounding condition leads to similar changes in sensitivities. It shows the potential of the proposed sensor for operation in differential mode that can eliminate the environmental effects. In this sensor, an SIW at ISM (Industrial Scientific and Medical) band is designed as a transmission line. The CSRRs are etched on top wall of SIW, that results in Transmission Zero (TZ) on transmission coefficient as well as size reduction. Therefore, loaded SIW operates below the characteristic cut off frequency of equivalent waveguide in evanescent mode. Finally, rectangular extension is connected to inner slot of CSRR. Therefore, the total slot length is increased and dual band operation is realized. The operation principle of the proposed sensor is based on TZs changes due to loading with MUT. The major points of the presented sensor can be summarized as follows:

- Dual band operation with one sensing area and with modified CSRRs
- The equal normalized theoretical sensitivity for both bands
- Compact size, because of inductive and capacitive effects of CSRRs loaded on empty space in top side of SIW
- High sensitivity due to increasing the electrical length of CSRRs with rectangular slot
- The easily integration with other planar components outcome of using SIW as host transmission line

The paper is organized as follows: design of SIW resonator is presented in details in Section II. Equivalent circuit model and sensitivity analysis is formulated as well. Section III presents measurement results and performance comparison with similar designs reported in the literature. Finally, section IV draws some conclusions.

II. DESIGN AND OPERATION PRINCIPLE

The configuration of the proposed sensor including an SIW and two CSRRs as host transmission line and sensing area are shown in Fig. 1. The electric field has maximum value in middle part of SIW according to waveguide operation principle [28]. Therefore, CSRRs are located in middle part of SIW, so that any perturbation in electric fields distribution leads to change in operation frequency and transmission zeros of the sensor. Loading the SIW with CSRRs results in a notch on transmission coefficient due to capacitive and inductive effects of CSRRs. A split rectangular slot inside the CSRRs generates second transmission zero that leads to dual notch behavior of the sensor. In the proposed sensor, size minimization is the motivation for using CSRRs on top of SIW, as one sensing area for dual band operation while two sensing parts are used in similar sensors. On the other hand, high sensitivity to permittivity can be achieved by extending the electrical length of CSRRs in rectangular form.

A. Design Procedure

SIW is realized with two rows of metallic vias on PCB. In the proposed sensor an SIW for operation in ISM band on RO4003 with $\epsilon_r = 3.55,\ tan\delta = 0.0027,\ h = 0.508$mm has been designed. The width of SIW found as in [29-30]:

$$W_{SIW} = W + \frac{d^2}{0.95P} \quad (1)$$

$$f_{c10} = \frac{1}{2W\sqrt{\mu\varepsilon}} \quad (2)$$

where d is the diameter of the vias, P is the pitch between adjacent vias, and W is the width of the equivalent rectangular waveguide. The values of d and P are set to minimize radiation loss as well as return loss. For an electrically small post $d < 0.2\lambda_{gSIW}$ minimum radiation loss is achieved. With $\frac{d}{P} \geq 0.5$ and $\frac{d}{W_{SIW}} < 0.4$ the SIW can perfectly map to equivalent rectangular waveguide [30]. For the proposed sensor P=1 mm, d=1.5 mm, $f_{c10} = 2.7\ GHz$ are selected and $W_{SIW} = 27.8\ mm$ is found from (1) and (2).

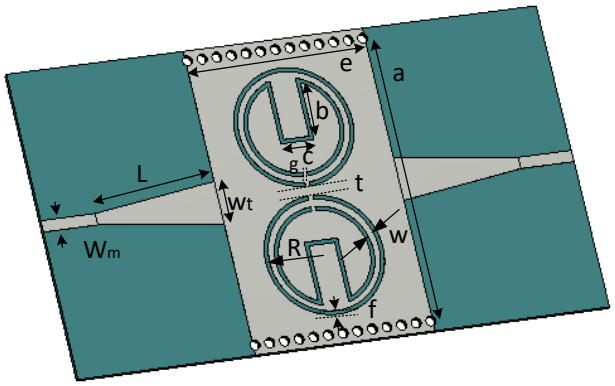

Fig. 1. The proposed sensor configuration, a=27.8mm, b=4.77mm, c=3.41mm, f=0.4mm, e=18.4mm, L=12.5, w=0.6mm, Wt=4.35mm, Wm=1.1mm, g=0.45mm, t=1mm, R=6mm.

The simulation result of the SIW is shown in Fig. 2 (a). Two sub wavelength CSRRs are aligned in the center of SIW in order to provide strong coupling between SIW and CSRRs [31] as the electric filed reaches maximum values in the waveguide center [32]. Fig. 2 (b) shows the simulation result of the loaded SIW. SIW was operating below the cut-off frequency [33] therefore operation frequency was shifted to a lower frequency at 1.2975 GHz. The miniaturization factor for the proposed SIW can be calculated as following.

$$M.F. = \frac{A_{SIW,f0} - A}{A_{SIW,f0}} \times 100 \qquad (3)$$

Where $A_{SIW,f0}$ and A are the area of conventional SIW at operation frequency of f_0 and the area of the proposed SIW loaded with CSRRs, respectively. The width of the SIW for the operation frequency of 1.2975 GHz is 61.36 mm according to (1) and for the proposed sensor in Fig.2 (b) is 27.8mm. Miniaturization factor is about 54.7% for the proposed sensor (3). Moreover, the first TZ is appeared according to Fig. 2 (b). The CSRRs can be viewed as electric dipole [34] and behave as electric scatterers. Therefore, CSRRs are capable of generating a stop band [35-36] and also evanescent-wave transmission. Split rectangular ring is connected to the inner ring of CSRR so, the electrical length of the proposed CSRR is longer than conventional CSRR. Therefore, the current passing through the gaps experiences an extra inductance. Consequently, another TZ is appeared, and also the first TZ is changed. Finally dual notch SIW sensor at 1.888GHz and 2.983GHz frequencies is achieved as shown in Fig. 2 (c). The effects of two geometrical parameters on the TZs locations are studied. The different length values of rectangular split ring (b) and gap of CSRRs (g) are examined, and the simulation results are shown in Fig. 3 and Fig. 4, respectively. By increasing the length of rectangular split ring (b) higher TZ frequency shifts up (Fig. 3(a)) whereas the lower TZ frequency shifts down (Fig. 3(b)). Fig. (2) shows that by increasing the length of rectangular split ring the electrical length and consequently the inductance effect due to lower TZ increases therefore, TZ becomes smaller. For the higher TZ by decreasing the corresponding electrical length, inductive effect decreases and TZ is growing. Increasing the gap (g) in the proposed sensor leads to increasing the higher and lower TZs according to Fig. 4. The simulation results in Fig.3 and Fig. 4 show that with these two parameters the TZs of the proposed sensor can be adjusted for desired band, and also dual notch operation is carried out, without changing the size of the structure.

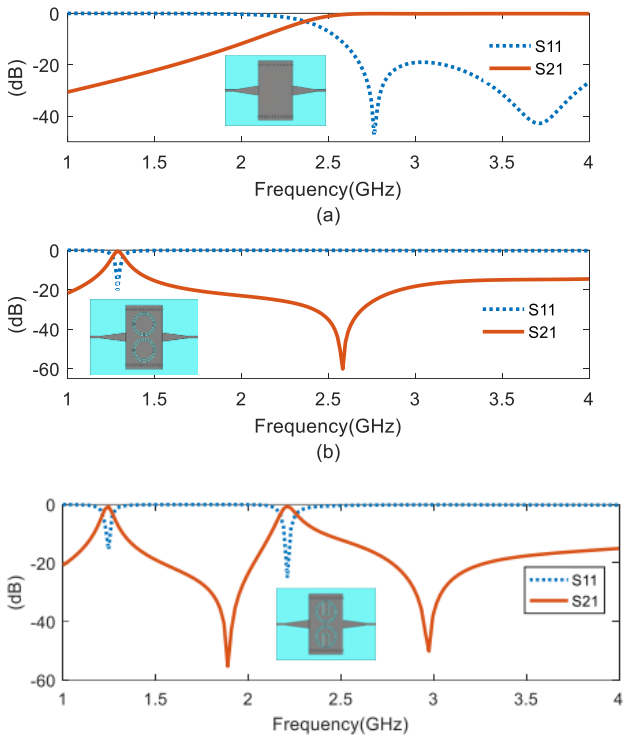

Fig. 2. The simulation results of (a) SIW (b) SIW loaded with CSRRs (c) SIW dual notch sensor.

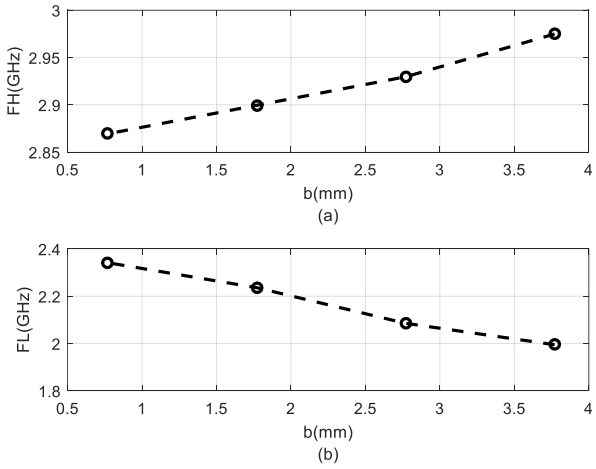

Fig. 3. The effect of rectangular split ring length on (a) high TZ (b) low TZ

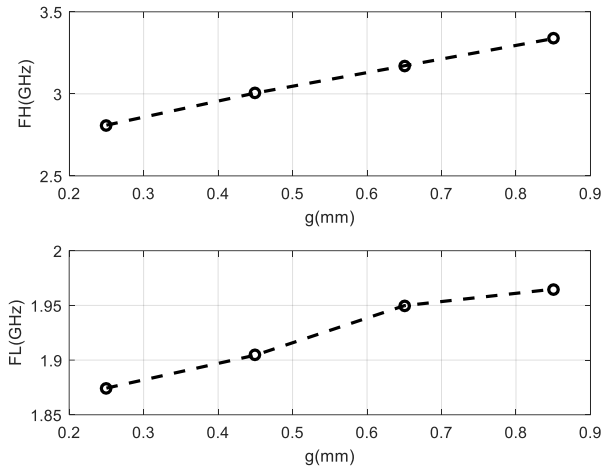

Fig. 4. The effect of gap on (a) high TZ (b) low TZ

B. Equivalent Circuit Model

The equivalent circuit model of the proposed sensor is derived for design purposes as shown in Fig. 5(a) [27]. The simulation results in Fig. 5(b) possesses two TZs and two poles. The first TZ is created from coupling between SIW and CSRRs. The second TZ is related to mutual coupling between modified CSRRs. The metalized via and CSRRs are modeled as L_d and shunt connected resonator tank formed by capacitance C_r and inductance L_r respectively. Inductive connection through the split of rings between the SIW and resonators, is shown with L_c. The capacitive coupling between the SIW and CSRRs is denoted by C_c. The magnetic and electric coupling between CSRRs is described by parallel combination of L_s and C_s. This circuit model is a simple version and it is valid for a restricted frequency range. The electrical parameters of the proposed model are, $L_d = 13.544$ nH, $L_c = 2.9155$ nH, $C_c = 2.44$ pF, $L_s = 0.5$ nH, $C_s = 5.75$ pF, $L_r = 2.1695$ nH, $C_r = 9.012$ pF. The equivalent circuit model gives first TZ at:

$$f_{ZL} = \frac{1}{2\pi\sqrt{L_c C_c}} \tag{4}$$

The second TZ is raised from coupling between CSRRs and it is given with:

$$f_{ZH} = \frac{1}{2\pi\sqrt{L_s C_s}} \tag{5}$$

Therefore, the initial values of circuit parameters (L_c, C_c, L_s, C_s) find from (4) and (5). The shunt connected resonator tank (L_r, C_r) create poles in transmission coefficient (Fig. 5(b)), so L_r *and* C_r extract from pole values. The extracted initial values for the equivalent circuit with the mentioned methodology are optimized in ADS software. In order to verify the circuit model, the simulation result of circuit and electromagnetic model are compared in Fig. 5 (b). Despite a small frequency shift in the second transmission pole, there is a good agreement between the results.

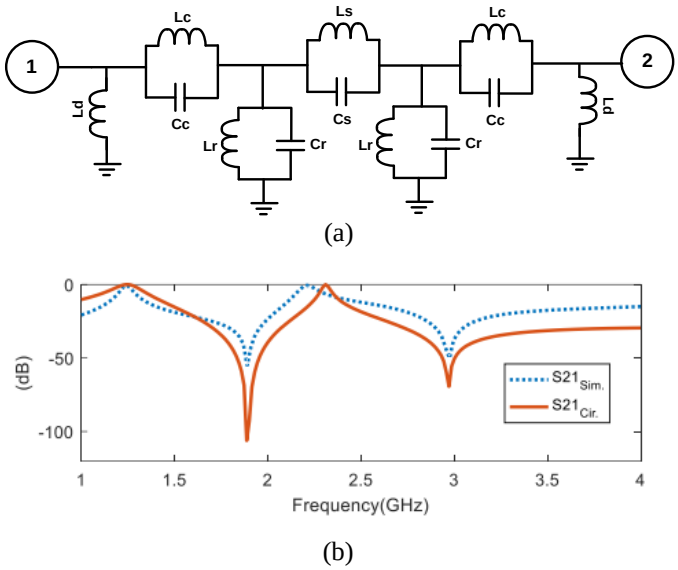

Fig. 5. (a) The equivalent circuit model. (b) the simulation results of the equivalent circuit model, and the electromagnetic model.

C. Sensitivity Analysis

The theoretical sensitivity analysis of the proposed sensor is carried out based on the simulation results of MUT for different permittivity values. In simulations, a glass with the size of 24×50× 0.13 mm^3 lies on the top of the CSRRs so that it covers CSRRs completely. The permittivity of cover glass ϵ_r is varied from 1 to 10 with steps of 1 in the simulation and TZs are recorded. Polynomial curve fitting model [37] is used for formulating, explicitly, the dependency of high and low TZs on the permittivity of MUT as shown in (6). The polynomial coefficients are listed in Table I.

$$f_{Zi} = \mathrm{a}_i \times 10^{-4}{\epsilon_r}^4 + \mathrm{b}_i \times 10^{-3}{\epsilon_r}^3 + \mathrm{c}_i \times 10^{-2}{\epsilon_r}^2 + \mathrm{d}_i \times 10^{-1}\epsilon_r + e_i \qquad i = H, L \tag{6}$$

TABLE I
Polynomial Model Coefficients

i	a_i	b_i	c_i	d_i	e_i
H	1.001	−2.94	3.428	−2.534	3.202
L	-0.537	1.659	1.980	-1.514	2.022

H=Higher L=Lower

The theoretical sensitivity is also derived from (7) [37].

$$S = \frac{\partial f_z}{f_o \partial \epsilon_r} \times 100 \tag{7}$$

Where f_z is the TZ and f_o is the TZ of the empty sensor, and ϵ_r is the relative permittivity of the load. High and low transmission zeros variation in terms of permittivity are shown in Fig. 7 (a) and (b) respectively. Higher transmission zeros show 825 MHz changes while low transmission zeros show 522 MHz changes for the same permittivity variation. The normalized sensitivity for low and high TZs is 3.1%. Therefore, any environmental conditions have the same effect on the sensitivity. The sensitivity variation in terms of the sample permittivity's is shown in Fig. 8(a) and Fig. 8(b) for high and

low TZs respectively. It shows that by increasing the permittivity, the sensitivity is decreased generally.

D. Thickness and Lift-off Analysis

The shift in transmission zeros of the proposed sensor can be explained as the interaction between fringing electric field of the CSRRs with the dielectric samples. This near field phenomenon is limited to very close proximities to CSRRs. The sample dimensions are selected so that, it covers whole CSRRs area and the sensitivity to position of samples is removed. However, the sensor is sensitive to thickness of the samples. In order to eliminate thickness effect, thick enough samples are used. In thin samples fringing fields are confined inside the sample volume. The minimum thickness which is enough for ignoring, the thickness effects is 1.4mm which, is find with simulation of a sample for different thicknesses [4]. In the proposed design, the fringing field decreases with increasing vertical distance. The simulation results show that the maximum lift-off distance is 0.6 mm and 0.4 mm for high and low TZs, respectively.

III. EXPERIMENTAL RESULTS

A prototype of the proposed sensor, is made and the measurement setup for permittivity characterization is provided. The measurement results including the TZs variation are used for experimental sensitivity computation.

A. Measurement Results

A prototype of the proposed SIW sensor is fabricated on RO4003 substrate. The measurement setup and fabricated SIW sensor are shown in Fig. 6. It includes the fabricated sensor, two clamps with plastic screws, an unmetallized PCB, and test samples. The sample under test is placed on top of the sensor. A piece of unmetallized PCB is placed under the sensor, and two clamps are holding the sample under test between its screws and sensor. The clamps keep the dielectric test samples in its position and push it against the substrate to achieve more accurate results. The test samples in rectangular shape with dimension of 20×30 mm^2 are cut from unmetallized microwave substrates. The size of the samples is adjusted for completely covering the sensing area of the sensor (CSRRs). The thickness of the samples is larger than 1.2 mm to neutralize the thickness effect on TZs of proposed sensor. Test samples are RT Duroid 5870($\epsilon_r = 2.33$ $h = 1.575$mm), FR4($\epsilon_r = 4.3$ $h = 1.6$ mm), RT Duroid 6006($\epsilon_r = 6$ $h = 1.905$ mm), RT Duroid 6010($\epsilon_r = 10.22$ $h = 1.9$ mm). The measured high and low TZs are summarized in TABLE II.

TABLE II
MEASUREMENT RESULTS FOR DIFFERENT SAMPLES

Sample	ϵ_r	High TZs(GHz)	Low TZs(GHz)
RT 5870	2.33	2.095	1.405
FR4	1.6	2.425	1.600
RT 6006	6	2.545	1.675
RT 6010	10.22	2.740	1.795
Bare	1	2.965	1.930

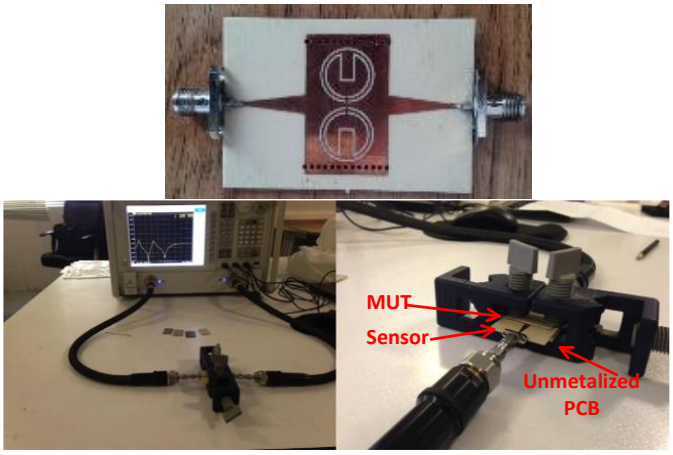

Fig. 6. The measurement setup and fabricated SIW sensor.

Measurement results for high and low TZs are shown in Fig. 7(a) and Fig. 7(b) respectively. The high frequency variation (645 MHz) is larger than low frequency (390 MHz) variation for the same permittivity difference, which is close agreement with simulation results. Polynomial curve fitting model are applied on the data in TABLE II [37] for obtaining the dependency of high and low TZs to permittivity of MUT as shown in (8) and TABLE III. The experimental sensitivity for high and low transmission zeros is extracted and shown in Fig. 8 (a) and (b) separately. Examining Fig. 8 reveals that sensitivity follows a similar trend.

$$f_{Zi} = \mathrm{a}_i \times 10^{-3}{\epsilon_r}^3 + \mathrm{b}_i \times 10^{-2}{\epsilon_r}^2 + \mathrm{c}_i \times 10^{-1}\epsilon_R + d_i \qquad i = H, L \tag{8}$$

TABLE III
Polynomial Model Coefficients

i	a_i	b_i	c_i	d_i
H	−7.846	1.837	−2.093	3.152
L	-6.194	1.331	-1.345	2.050

H=Higher L=Lower

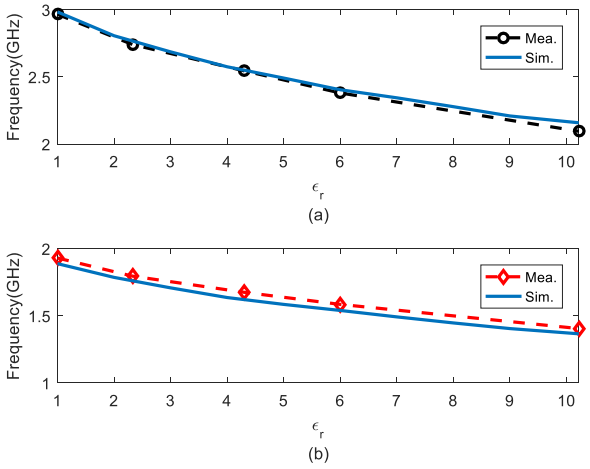

Fig. 7. Measured and simulation transmission zeros as a function of permittivity for (a) high TZ (b) low TZ

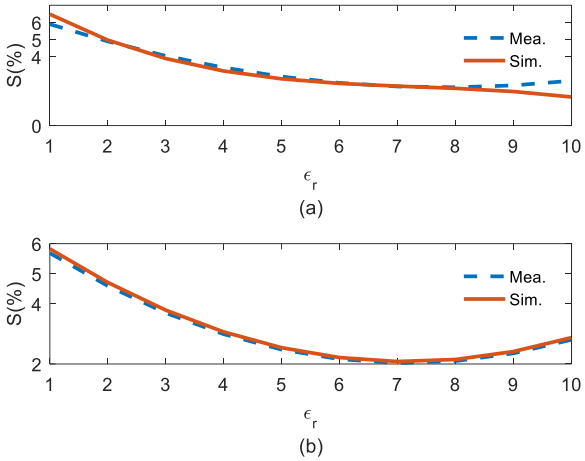

Fig. 8 Measured and simulation sensitivity as a function of loaded sample permittivity (a) Higher TZ (b) Lower TZ

detection frequency domain, respectively. The size of SIW part of the sensor without microstrip transition part is shown with A_{SIW}. Therefore, the size reduction effect due to inductive and capacitive effects of CSRRs is included. By considering the different operation frequency of the sensors, its size must be normalized for fair comparison. So, A_{SIW} (λ_g^2) (the normalized size to guided wavelength of SIW) is shown in TABLE IV. The guided wavelength for equivalent rectangular waveguide is given by:

$$\lambda_g = \frac{\lambda}{\sqrt{1-(\frac{f_c}{f_o})^2}} \tag{11}$$

Where f_c and f_o are given in (2) and (10) respectively and λ is the operation wavelength. Normalized size of the proposed sensor is 0.05 and 0.1 with respect to high and low TZs respectively. Comparison table shows that the size of the

TABLE IV
COMPARISON OF THE PROPOSED SENSOR WITH OTHER SENSORS

Ref.	f_0 (GHz) Upper	Lowe	$\frac{\Delta f}{\Delta \epsilon_r}(MHz)$	S (%)	A_{SIW} (λ_g^2)	Material type	R.P	Sensor Type
[6]	5.831(5.812-5.850)	-	0.6	1.03×10^{-2}	0.51	Liquid	8-70	Slot in SIW
[11]	2.455(2.391-2.519)	-	1.77	7.2×10^{-2}	0.25	Liquid	5.25-77.5	Hole in SIW
[18]	2.674(2.673-2.677)	-	0.63	2.7×10^{-3}	0.214	Liquid	4.78-39.19	I.C in SIW
[15]	2.977(2.897-3.058)	-	20.18	0.67	0.23	Solid	2.1-10.2	Slot in SIW
[38]	2.5	-	-	0.27	0.07	Liquid	1-140	SRR
Proposed	2.4175(2.095-2.740)	1.6(1.405-1.795)	49.43-81.75	3.4-3.1	0.05-0.1	Solid	2.33-10.22	CSRRs in SIW

R.P=Range of permittivity in measurement, I.C=Interdigital Capacitance

The measurement results in TABLE II are used for comparing the proposed sensor with similar structures. Most of the selected designs in TABLE IV have made on SIW technology. To make more inclusive comparison some sensors which are made with microstrip and SRR are investigated. SRR in folded form for liquid characterization [38] and in parallel form for monitoring the flowing fluids inside a capillary [39] are used. Non-invasive glucose sensing in aqueous solution with an active SRR is also reported [40]. For having the reasonable comparison, the normalized sensitivity is used as follows.

$$S = \frac{1}{f_o}\frac{\Delta f}{\Delta \epsilon_r} \times 100 \tag{9}$$

$$f_0 = \frac{f_{01}+f_{02}}{2} \qquad \Delta f = f_{o2} - f_{o1} \tag{10}$$

where f_{o1} and f_{o2} are upper and lower frequencies in proposed sensor is at least 4 times less than similar SIW sensor in high TZ and close to [38]. Moreover, the normalized sensitivity is 3.4 and 3.1 percent for high and low TZs respectively. These sensitivity values are close and confirms the differential mode operation of proposed sensor. The normalized sensitivity of proposed sensor is 5 times greater than the best of the similar sensors. Range of permittivity for liquid MUT is higher than solid MUT.

IV. Conclusion

A new SIW based sensor for material characterization is proposed. SIW and CSRRs are used as host and sensing area respectively. CSRRs are etched on middle part of SIW surface, to reach extreme coupling. The proposed sensor operates bellow cut off frequency and has two TZs. Experimental results show 3.4% and 3.1% normalized sensitivity for high and low TZs respectively. The normalized size of the SIW which includes sensing area are 0.05 and 0.1 for high and low TZs. Comparison

table show high sensitivity and small size of the proposed sensor with respect to similar structures.

REFERENCES

[1] M. Schueler, C. Mandel, M. Puentes and R. Jakoby, "Metamaterial Inspired Microwave Sensors," in IEEE Microwave Magazine, vol. 13, no. 2, pp. 57-68, March-April 2012, doi: 10.1109/MMM.2011.2181448.

[2] Amir Ebrahimi, James Scott, Kamran Ghorbani, "Microwave reflective biosensor for glucose level detection in aqueous solutions," Sensors and Actuators A: Physical, Volume 301, 2020, 111662, ISSN 0924-4247,

[3] A. Ebrahimi, W. Withayachumnankul, S. Al-Sarawi, and D. Abbott, "High-sensitivity metamaterial-inspired sensor for microfluidic dielectric characterization, " IEEE Sensors Journal, vol. 14, no. 5, pp. 1345–1351, May 2014.

[4] A. Ebrahimi, J. Scott, and K. Ghorbani, "Differential sensors using microstrip lines loaded with two split ring resonators, " IEEE Sensors Journal, vol. 18, no. 14, pp. 5786–5793, July 2018.

[5] A. Ebrahimi, J. Scott and K. Ghorbani, "Dual-Mode Resonator for Simultaneous Permittivity and Thickness Measurement of Dielectrics," in IEEE Sensors Journal, vol. 20, no. 1, pp. 185-192, 1 Jan.1, 2020, doi: 10.1109/JSEN.2019.2941753.

[6] C. Liu and F. Tong, "An SIW Resonator Sensor for Liquid Permittivity Measurements at C Band," in IEEE Microwave and Wireless Components Letters, vol. 25, no. 11, pp. 751-753, Nov. 2015, doi: 10.1109/LMWC.2015.2479851.

[7] E. Silavwe, N. Somjit and I. D. Robertson, "A Microfluidic-Integrated SIW Lab-on-Substrate Sensor for Microliter Liquid Characterization," in IEEE Sensors Journal, vol. 16, no. 21, pp. 7628-7635, Nov.1, 2016, doi: 10.1109/JSEN.2016.2599099.

[8] P. Mohammadi and S. Demir, "Multi-layer substrate integrated waveguide E-plane power divider", Progress Electromagn. Res. C, vol. 30, pp. 159-172, June 2012.

[9] P. Mohammadi, S. Demir, "Loss reduction in substrate integrated waveguide structures", Progr. Electromagnet. Res. 46 (2014) 125–133.

[10] N. K. Tiwari, A. K. Jha, S. P. Singh, Z. Akhter, P. K. Varshney and M. J. Akhtar, "Generalized Multimode SIW Cavity-Based Sensor for Retrieval of Complex Permittivity of Materials," in IEEE Transactions on Microwave Theory and Techniques, vol. 66, no. 6, pp. 3063-3072, June 2018, doi: 10.1109/TMTT.2018.2830332.

[11] E. Massoni, G. Siciliano, M. Bozzi and L. Perregrini, "Enhanced Cavity Sensor in SIW Technology for Material Characterization," in IEEE Microwave and Wireless Components Letters, vol. 28, no. 10, pp. 948-950, Oct. 2018, doi: 10.1109/LMWC.2018.2864876.

[12] Tan, Q.; Guo, Y.; Zhang, L.; Lu, F.; Dong, H.; Xiong, J. "Substrate Integrated Waveguide (SIW)-Based Wireless Temperature Sensor for Harsh Environments". Sensors 2018,18, 1406.

[13] S. Chen et al., "A Dielectric Constant Measurement System for Liquid Based on SIW Resonator," in IEEE Access, vol. 6, pp. 41163-41172, 2018, doi: 10.1109/ACCESS.2018.2857514.

[14] A. Benleulmi, N. Y. Sama, P. Ferrari and F. Domingue, "Substrate Integrated Waveguide Phase Shifter for Hydrogen Sensing," in IEEE Microwave and Wireless Components Letters, vol. 26, no. 9, pp. 744-746, Sept. 2016, doi: 10.1109/LMWC.2016.2597177.

[15] P. K. Varshney and M. J. Akhtar, "Permittivity Estimation of Dielectric Substrate Materials via Enhanced SIW Sensor," in IEEE Sensors Journal, vol. 21, no. 10, pp. 12104-12112, 15 May15, 2021, doi: 10.1109/JSEN.2021.3064923.

[16] Taehwa Yun, Sungjoon Lim, "High-Q and miniaturized complementary split ring resonator-loaded substrate integrated waveguide microwave sensor for crack detection in metallic materials, "Sensors and Actuators A: Physical, Volume 214, 2014, Pages 25-30,

[17] P. K. Varshney and M. J. Akhtar, "Substrate Integrated Waveguide Derived Novel Two-Way Rotation Sensor," in IEEE Sensors Journal, vol. 21, no. 2, pp. 1519-1526, 15 Jan.15, 2021, doi: 10.1109/JSEN.2020.3017622.

[18] H. Lobato-Morales, J. H. Choi, H. Lee and J. L. Medina-Monroy, "Compact Dielectric-Permittivity Sensors of Liquid Samples Based on Substrate-Integrated-Waveguide With Negative-Order-Resonance," in IEEE Sensors Journal, vol. 19, no. 19, pp. 8694-8699, 1 Oct.1, 2019, doi: 10.1109/JSEN.2019.2922137.

[19] D. Covarrubias-Martínez, O. A. Martínez-Rodríguez, H. Lobato-Morales and J. L. Medina-Monroy, "Classification of Plastic Materials using a Microwave Negative-Order-Resonance Sensor and Support-Vector-Machine," 2021 96th ARFTG Microwave Measurement Conference (ARFTG), 2021, pp. 1-4, doi: 10.1109/ARFTG49670.2021.9425184.

[20] M. Abdolrazzaghi, S. Khan and M. Daneshmand, "A Dual-Mode Split-Ring Resonator to Eliminate Relative Humidity Impact," in IEEE Microwave and Wireless Components Letters, vol. 28, no. 10, pp. 939-941, Oct. 2018, doi: 10.1109/LMWC.2018.2860596.

[21] M. A. H. Ansari, A. K. Jha, and M. J. Akhtar, "Dual band microwave sensor for dielectric characterization of dispersive materials," in Proc. Asia–Pacific Microw. Conf. (APMC), Dec. 2016, pp. 1–3.

[22] A. A. Abduljabar, N. Clark, J. Lees, and A. Porch, "Dual mode microwave microfluidic sensor for temperature variant liquid characterization," IEEE Trans. Microw. Theory Techn., vol. 65, no. 7, pp. 2572–2582, Jul. 2017.

[23] T. Haq, C. Ruan, S. Ullah and A. Kosar Fahad, "Dual Notch Microwave Sensors Based on Complementary Metamaterial Resonators," in IEEE Access, vol. 7, pp. 153489-153498, 2019, doi: 10.1109/ACCESS.2019.2948868.

[24] L. Su, J. Mata-Contreras, P. Velez, and F. Mart ´ ´ın, "Splitter/combiner microstrip sections loaded with pairs of complementary split ring resonators (CSRRs): modeling and optimization for differential sensing applications," IEEE Trans. Microw. Theory Techn., vol. 64, no. 12, pp. 4362–4370, 2016

[25] P. Velez, L. Su, K. Grenier, J. Mata-Contreras, D. Dubuc, and F. Martin, "Microwave microfluidic sensor based on a microstrip splitter/combiner configuration and split ring resonators (SRRs) for dielectric characterization of liquids," IEEE Sensors Journal, vol. 17, no. 20, pp. 6589–6598, 2017.

[26] J. Naqui, C. Damm, A. Wiens, R. Jakoby, L. Su, J. Mata-Contreras, and F. Mart´ın, "Transmission lines loaded with pairs of stepped impedance resonators: modeling and application to differential permittivity measurements," IEEE Trans. Microw. Theory Techn., vol. 64, no. 11, pp. 3864–3877, 2016.

[27] Y. D. Dong, T. Yang and T. Itoh, "Substrate Integrated Waveguide Loaded by Complementary Split-Ring Resonators and Its Applications to Miniaturized Waveguide Filters," in IEEE Transactions on Microwave Theory and Techniques, vol. 57, no. 9, pp. 2211-2223, Sept. 2009, doi: 10.1109/TMTT.2009.2027156.

[28] David M. Pozar, "Microwave Engineering," *3rd ed.* Wiley, *2005.*

[29] P. Mohammadi, R Gheibi, "A new design of substrate integrated waveguide diplexer using complementary split ring resonators," International Journal of RF and Microwave Computer-Aided Engineering, vol. 29 no. 8 pp. 1-5, 11 April 2019, doi.org/10.1002/mmce.21772.

[30] Deslandes D, Wu K. "Single-substrate integration technique of planar circuits and waveguide filters," IEEE Trans Microwave Theory Techn. 2003;51(2):593-596

[31] Mostafa Danaeian, Kambiz Afrooz, Ahmad Hakimi, "Miniaturization of substrate integrated waveguide filters using novel compact metamaterial unit-cells based on SIR technique", AEU - International Journal of Electronics and Communications, Volume 84, 2018, Pages 62-73.

[32] Dong, Y., C.-T. M. Wu, and T. Itoh, "Miniaturised multi-band substrate integrated waveguide filters using complementary split-ring resonators," IET Microw. Antennas Propag., Vol. 6, No. 6, 611-620, 2012. doi:10.1049/iet-map.2011.0448

[33] Y. Dong and T. Itoh, "Substrate Integrated Waveguide Loaded by Complementary Split-Ring Resonators for Miniaturized Diplexer Design," in IEEE Microwave and Wireless Components Letters, vol. 21, no. 1, pp. 10-12, Jan. 2011, doi: 10.1109/LMWC.2010.2091263.

[34] J. D. Baena, J. Bonache, F. Martin, R. Marques, F. Falcone, T. Lopetegi, M. A. G. Laso, J. Garcia, I. Gil, and M. Sorolla, "Equivalent-circuit models for split-ring resonators and complementary split-ring resonators coupled to planar transmission lines, " IEEE Trans. Microw. Theory Tech., vol. 53, no. 4, pp. 1451–1461, Apr. 2005.

[35] X. Zhang, Z. Yu, and J. Xu, "Novel band-pass substrate integrated waveguide filter based on complementary split ring resonators, " Progr. Electromagn. Res., vol. 72, pp. 39–46, 2007.

[36] W. Che, C. Li, K. Deng, and L. Yang, "A novel bandpass filter based on complementary split rings resonators and substrate integrated waveguide," Microw. Opt. Technol. Lett., vol. 50, no. 3, pp. 699–701, Nov.

[37] P. Mohammadi, A. Mohammadi, S. Demir and A. Kara, "Compact Size, and Highly Sensitive, Microwave Sensor for Non-Invasive Measurement of Blood Glucose Level," in IEEE Sensors Journal, vol. 21, no. 14, pp. 16033-16042, 15 July15, 2021, doi: 10.1109/JSEN.2021.3075576.

[38] M. Abdolrazzaghi, M. Daneshmand and A. K. Iyer, "Strongly Enhanced Sensitivity in Planar Microwave Sensors Based on Metamaterial Coupling," in IEEE Transactions on Microwave Theory and Techniques, vol. 66, no. 4, pp. 1843-1855, April 2018, doi: 10.1109/TMTT.2018.2791942.

[39] M. Abdolrazzaghi and M. Daneshmand, "Dual Active Resonator for Dispersion Coefficient Measurement of Asphaltene Nano-Particles," in IEEE

Sensors Journal, vol. 17, no. 22, pp. 7248-7256, 15 Nov.15, 2017, doi: 10.1109/JSEN.2017.2734692.
[40] M. Abdolrazzaghi, N. Katchinskiy, A. Elezzabi, P. E. Light and M. Daneshmand, "Noninvasive Glucose Sensing in Aqueous Solutions Using an Active Split-Ring Resonator," in IEEE Sensors Journal, doi: 10.1109/JSEN.2021.3090050.

Pejman Mohammadi, received Ph.D. in Electrical Engineering from the Middle East Technical University Turkey. Since 2001, he has been with the Department of Electrical Engineering, Islamic Azad University of Urmia, Iran where he is currently Associate Professor. His research interests include microwave component SIW, microstrip antennas, small antennas for wireless communications, and reconfigurable structures.

Dr Ali Mohammadi, received PhD degree in Electrical Engineering from the University of Newcastle Australia (2014). He conducted post-doctoral research at Monash University and University of Oxford. He is a lecturer (Assistant Professor) at the Department of Electronics and Electrical Engineering, University of Bath, UK. His research interests include microelectromechanical (MEM) devices and microelectronic circuits with applications in micro-energy harvesting and high precision sensing. Dr Mohammadi received MEMS Design Awards form Europractice completions in 2018 and 2020.

Simsek Demir(S'91–M'98) received the B.Sc.,M.Sc., and Ph.D. degrees in electrical and electronics engineering from Middle East Technical University (METU), Ankara, Turkey, in 1991, 1993, and1998, respectively. From 1991 to 1998, he was a Research Assistant with METU. From 1998 to 1999, he contributed to the atmospheric radar antenna design with IRCTR,TU-Delft, The Netherlands. Since 2000, he has been a Professor with the Electrical and Electronics Engineering Department, METU. His current research interests include microwave and millimeter-wave active and passive components, and system design, analysis, and modeling. His research topics include the exploitation of RF MEMS technology toward industrial use, power amplifier design, modeling and implementation, and radar applications.

Ali Kara received Ph.D. degree from Hacettepe University in 2002. He was with Polytechnic University (ECE), Brooklyn, from 1999 to 2000, where he conducted theoretical and experimental research. He joined the Department of Electrical and Electronics Enginering of Atilim University, in 2000 and worked until 2021, where he held various positions ranging from lecturer to full professor levels. As of April 2021, he joined the Department of Electrical and Electronics Engineering, Gazi University. He has published extensively in Electromagnetics, Antennas and Propagation as well as Engineering Education. He has four patents, and has led several national and international projects.